A computational method for combustion in high speed flows

C. Ferrat, R. Marsilio *

Department of Mechanical and Aerospace Engineering, Politecnico di Torino, Corso Duca degli Abruzzi, 24, 10129 Torino, Italy

A B S T R A C T

A two-dimensional time-accurate numerical model to simulate complex reacting flowfields in chemical non-equilibrium is presented. The aim of this study is to develop a computational tool which permits the analysis and the easy implementation of combustion phenomena for high speed flows. To construct an efficient numerical tool, while maintaining a reasonable accuracy, a semi-implicit numerical method was selected and verified for a hydrogen–air mixture. The numerical approach is based on a time-dependent, finite volume integration of the governing equations suitably modified for chemical non-equilibrium. The evaluation of the reacting constants based on Gibbs free energy and the Van't Hoff equation allows a very easy implementation of the chemical model used, regardless of its complexity. Calculations were performed with adeguate temporal and spatial resolution for modeling the physical process for practical calculation. Comparisons with numerical results are used for a verification of the numerical procedure.

1. Introduction

Computational Fluid Dynamics (CFD) has grown rapidly in the past 25 years and is now an important tool for analyzing and understanding complex fluid flows. CFD has played a vital role in the study of hypersonic flight. It has provided the capability for scientists and engineers to model both internal and external hypersonic flow fields. These flows are often impractical or impossible to analyze in laboratory conditions. In particular, the recent application of CFD to the modeling of internal reacting supersonic combustor flows has significantly advanced the understanding of such flows and has increased confidence in the predictive ability of codes. The purpose of these efforts has been to provide the hypersonic propulsion community with realistic large-scale applications of CFD and to use these solutions as a direct means of support for the engineering analysis and design of hypersonic vehicles. Although these applications have been successful to date, expectations and requirements are increasing dramatically for both faster turn-around of solutions and for more detailed and accurate solutions (hence requiring a greater computational mesh refinement, more complete chemistry and turbulence models, etc.). In order to meet few of these requirements, a numerical code based on Euler equations formulated in conservative form and coupled with a complex chemical reaction kinetic model has been developed for two-dimensional reacting flows to study unsteady high speed flow combustion phenomena.

* Corresponding author.
E-mail addresses: ferrat.christian@hotmail.it (C. Ferrat), roberto.marsilio@polito.it (R. Marsilio).

The analysis of unsteady combustion phenomena has been carried out as a case-study. In particular, the attention has been focused on the study of a detonation based, multi-mode, single-path propulsion system, proposed for space access or hypersonic cruise [1–3].

Wedge and cone-induced oblique shock/detonation waves have received wide-spread attention to their potential application in hypersonic propulsion device. These include ram accelerator [4], and oblique detonation wave engine [5–7]. These above cited studies were concerned with the body in a semi-infinite domain. Generally, the numerical studies showed two possible ways that a detonation is achieved. In the first, an attached oblique shock in the incoming premixed combustible mixture transitions to a detonation, arising from the compression. In the second, a direct initiation is obtained. Under certain conditions, a stable wave system is not achieved. Moreover, complex wave interactions are expected when the wedge is confined in a channel. Such a confined wedge configuration appears to be more realistic in simulating the flow of a ram accelerator or an oblique shock detonation wave engine. The intrinsic unsteadiness of the confined detonation flow and its capability to induce detonation waves is the interest of the present study.

Depending on the flight Mach number, two working modes are possible: the normal detonation wave engine mode (NDWE) and the oblique detonation wave engine mode (ODWE) [3]. Witenberger and Shepherd [8] had previously concluded that a steady normal detonation wave cannot be established, thus the NDWE is, in fact, an unsteady propulsion concept. The NDWE is similar to the scramjet, except for the use of pulsed detonation rather than deflagration burning. The mixture equivalence ratio

can be used as a measure to control detonation wave behavior [2]. In the right conditions, a supersonic combustible mixture can be ignited by the shock induced by a sharp wedge, thereby dispensing with an external ignition system, avoiding premature upstream combustion. As reported in [3] the working process for the pulsed NDWE mode can be summarized as follows: fuel injection, detonation initiation at the wedge, normal detonation wave propagating upstream, fuel injection cutoff at the proper instant when maximum thrust has been obtained, purging, and start of next cycle.

In this situation the flow field could not be considered in chemical equilibrium and, as a consequence, there is a redistribution of energy among energy degrees of freedom, due to particle collision, which takes a certain time to occur. This phase is the so-called "relaxing time". Therefore, there are two relevant temporal scales dominating the phenomena: the first, τ_{ch} , is the temporal scale used to measure the temporal evolution of the chemical process, which is, referring to a simplified gas kinetic theory where p and T are the static pressure and the static temperature, respectively. The second, t_{fd} , represents the time needed by a fluid element to cross the entire flow field. This time can be easily evaluated as the rate between a characteristic dimension of the body L_{ref} and the referring fluid dynamic velocity u_{ref} . As occurs in a NDWE, the two previously mentioned times are of the same order of magnitude, therefore the relaxing process and the fluid dynamics evolve along the same timescale.

A simplified two-dimensional symmetric wedged domain is adopted for this study. This configuration is used to capture the main process in a real pulsed NDWE mode. The physical phenomena are numerically modeled with an upwind time-dependent integration of a modified set of Euler equations, coupled with an appropriate combustion chemical model. A number of mass conservation equations have been added in the number of species, while energy equation has been modified in order to consider the variation of the pressure coefficient during the reaction process and to take into account the heat of formation of each species.

The system is discretized according to a finite volume technique. The convective part of the equations is dealt with using a flux difference splitting method with an approximate solution of a Riemann problem at each interface [9]. Second-order accuracy is achieved following the guidelines of the essentially non-oscillatory schemes (ENO), with linear reconstruction of the solu-tion inside each cell and at each step of integration [10]. Moreover, the conservative integration of the governing equations is able to capture any flow discontinuity, i.e. shocks and contact surfaces, that can occur in a supersonic combustion process. The implemented method for the calculation of the reaction rate constants is based on Gibbs free energy and the Van't Hoff equation, allowing an easy implementation and modification of the chemical model with no theoretical restriction on number of species and number of considered reactions [11].

A reduced mechanism for hydrogen and air combustion has been used to test the method. The chemical model is based on seven species $(H, O, OH, O_2, H_2, H_2O and N_2)$ and thirty-two reactions where the species HO_2 and H_2O_2 have been neglected and the N_2 is counted as a collisional partner in the thermodynamic model and in the relaxation process [12]. Numerical results are compared and discussed with those reported in [3].

2. Governing equations

The time-dependent two-dimensional Euler equations are used to described an inviscid, non-heat-conducting, reacting flow in vibrational equilibrium. This set of equations may be written in a compact integral conservative form as:

$$\frac{\partial}{\partial t}\int_{\mathcal{V}} \boldsymbol{W} d\mathcal{V} + \int_{\mathcal{S}} \boldsymbol{F}_I \cdot n d\mathcal{S} = \int_{\mathcal{V}} \boldsymbol{\Omega} d\mathcal{V} \tag{1}$$

where $\mathcal{V}$ represents an arbitrary volume enclosed in a surface $\mathcal{S}$. System (1) is reduced to non-dimensional form with the help of the following reference values: L_{ref} for length, ρ_∞ for density, T_∞ for temperature, $v_{ref} = \sqrt{R_{ref} T_\infty}$ for velocity, $t_{ref} = L_{ref}/v_{ref}$ for time, $R_{ref} T_\infty$ for energy per unit mass. The source terms have been converted to dimensionless values by $\Omega_{ref} = \rho_\infty / t_{ref}$. In particular, $\boldsymbol{W}$ is the vector of conservative variables, tensor $\boldsymbol{F}_I$ contains the inviscid fluxes and $\boldsymbol{\Omega}$ is the vector of source terms (chemical production terms).

$$\begin{aligned} &\boldsymbol{W} = \{\rho_i, \rho\boldsymbol{V}, E\}^T \\ &\boldsymbol{F}_I = \{\rho_i \boldsymbol{V}, p\boldsymbol{I} + \rho \boldsymbol{V} \otimes \boldsymbol{V}, (E+p)\boldsymbol{V}\}^T \\ &\boldsymbol{\Omega} = \{\Omega_i, \boldsymbol{0}, \boldsymbol{0}, 0\} \end{aligned} \tag{2}$$

The subscript $i = 1, 2, 3, \ldots, N_s$, where N_s is the number of species. The first N_s rows represent species continuity. Quantity ρ_i, is the density of i-species, $\rho = \sum_{i=1}^{N_s} \rho_i$ is the mixture density, p is the pressure, $\boldsymbol{V} = \{u, v\}^T$ is the velocity vector with cartesian components u and v, and Ω_i is the mass production rate of i-species per unit volume. E is the total energy per unit mass of mixture:

$$E = \rho\left(e + \frac{\boldsymbol{V}^2}{2}\right) = \rho\left(h - \frac{p}{\rho} + \frac{\boldsymbol{V}^2}{2}\right) \tag{3}$$

where h is the static enthalpy of the mixture. Being Y_i the mass fraction and μ_i the molecular mass of the i-species, the equation of state is given by:

$$\frac{p}{\rho} = \mathcal{R} T \sum_{i=1}^{N_s} \frac{Y_i}{\mu_i} \tag{4}$$

where $\mathcal{R} = 8.314 \mathrm{J/(mol\ K)}$ is the universal gas constant. The enthalpy is related to the temperature and to the overall heat of formation (h_{for}):

$$h = h_{for} + \sum_{i=1}^{N_s} c_{p_i} Y_i T \tag{5}$$

where

$$h_{for} = \sum_{i=1}^{N_s} y_i h_i^0 \tag{6}$$

and

$$\begin{aligned} c_{p_i} &= \frac{5}{2}\frac{\mathcal{R}}{\mu_i} \quad \text{monoatomic gas} \\ c_{p_i} &= \frac{7}{2}\frac{\mathcal{R}}{\mu_i} \quad \text{biatomic gas} \\ c_{p_i} &= \frac{8}{2}\frac{\mathcal{R}}{\mu_i} \quad \text{poliatomic gas} \end{aligned} \tag{7}$$

where h_i^0 and c_{p_i} are the standard enthalpy of formation and the specific heat at constant pressure of the i-species, respectively.

2.1. Chemical equations

In this section, a general method to obtain the rate of production terms for a chemical process of N_s species governed by M_s reactions will be explained and discussed.

A reacting flow in chemical non-equilibrium is characterized by continuous chemical production. Due to their mutual influence, in these conditions the non-equilibrium process and the variation of fluid dynamics variables cannot be decoupled. Therefore, for the study of a flow in chemical non-equilibrium it is necessary to

introduce the chemical rate equations which allow the source terms Ω_i in (1) to be computed [13,14]. The rate of production of the species (Ω_i) depends on local properties (p, ρ) and concentrations (Y_i):

$$\Omega_i = \Omega_i(p, \rho, Y_i) \tag{8}$$

The non-equilibrium mechanism of a reacting gas mixture can be constituted by many reactions among the existing species. In gen-eral, each reaction can progress simultaneously both in the direct direction, determining the passage from the reactants to the prod-ucts, and in the inverse one, from the products to the reactants. In a mixture of reacting gas all the M_s-reactions that can be chosen to define the chemical non-equilibrium mechanism combine, or may combine, into the production of the considered i-species. The overall production velocity of that species becomes, [13]:

$$\Omega_i = \mu_i \sum_{j=1}^{M_s} (\nu_i^r - \nu_i^l) K_{frd_j} \left[\prod_{i=1}^{N_s} (q_i)^{\nu_{i,j}^l} - \frac{1}{K_{eq_j}} \prod_{i=1}^{N_s} (q_i)^{\nu_{i,j}^r} \right] \tag{9}$$

It is therefore evident that the solution of the production Eq. (9) requires the elementary process determining the non-equilibrium mechanism of the gas mixture under exam to be identified and constants K_{frd_j} and K_{bkd_j} or constants K_{frd} and K_{eq} for each involved reaction to be defined. Constants K_{frd_j} are generally determined experimentally. The empirical results obtained can be correlated using the Arrhenius equation or its modified form, such as the following:

$$K_{frd_j} = CT^{\eta} e^{-\frac{\epsilon_0}{RT}} \tag{10}$$

The terms C, η and ϵ_0 are experimental coefficients that do not depend on temperature. The activation energy, ϵ_0, may be defined as the minimum energy required to start a chemical reaction. The described results for the chemical kinetic have been obtained for a closed system, with assigned temperature and volume, where only homogeneous reactions take place. The use of those equations for a flow, which is an open system with volume and temperature variations, can be justified, assuming that the chemical non-equilibrium relations are based on the instantaneous values of temperature and volume.

2.2. Calculation of the equilibrium constant: Gibbs free energy

The problem of calculation of the equilibrium constant for a chemical process becomes relevant in the absence of a model that can predict its value by using a certain interpolator polynomial based on experimental data. In this case, or when a general behavior for the solving process is needed, a way to calculate that constant using some known properties of the species which are involved in each chemical reaction must be found. It is necessary to introduce the state function called Gibbs free energy G:

$$G = H - TS \tag{11}$$

where H, S and T are the enthalpy, the entropy and the static temperature, respectively. In the case of reaction in equilibrium a relation between ΔG^0 (the variation of the Gibbs free energy in a standard condition) and the thermodynamic constant K can be obtained [11]:

$$\Delta G^0 = -RT \ln K \tag{12}$$

hence, K:

$$K = e^{-\frac{\Delta G^0}{RT}} \tag{13}$$

Most reactions do not start with all the reaction components in their standard state, so in order to calculate the equilibrium constant in a generic condition it is possible to use the Van't Hoff equation [11]:

$$K_2 = K_1 e^{\frac{\Delta H^0}{R}\left(\frac{1}{T_1} - \frac{1}{T_2}\right)} \tag{14}$$

With this equation, the equilibrium constant K_2 at a temperature T_2 of interest, can be computed if the equilibrium constant K_1 at temperature T_1 is known (the standard one). Since in literature the forward constant K_{frd} of a certain reaction is expressed in cm^3/(mol s) it is necessary to convert the equilibrium constant, Eq. (13), in order to make it consistent with the species concentration, and not with their partial pressure. As a consequence, the equilibrium constant may be written as:

$$K_{eq} = \frac{K}{(RT)^{c+d-a-b}} \tag{15}$$

3. Numerical method

The numerical approach presented is based on a time-dependent integration of the governing equations. For two-dimensional unsteady flow systems, Eq. (1), may be reduced as:

$$\frac{\partial}{\partial t} \int_{\mathcal{V}} \boldsymbol{W} d\mathcal{V} + \int_{\mathcal{S}} \boldsymbol{F} n_x d\mathcal{S} + \int_{\mathcal{S}} \boldsymbol{G} n_y d\mathcal{S} = \int_{\mathcal{V}} \boldsymbol{\Omega} d\mathcal{V} \tag{16}$$

where vectors $\boldsymbol{W}$, $\boldsymbol{F}$, $\boldsymbol{G}$ and $\boldsymbol{\Omega}$ may be written as:

$$\boldsymbol{W} = \begin{Bmatrix} \rho_i \\ \rho u \\ \rho v \\ E \end{Bmatrix} \quad \boldsymbol{F} = \begin{Bmatrix} \rho_i u \\ (p + \rho u^2) \\ \rho u v \\ (p + E) u \end{Bmatrix} \quad \boldsymbol{G} = \begin{Bmatrix} \rho_i v \\ \rho u v \\ (p + \rho v^2) \\ (p + E) v \end{Bmatrix} \quad \boldsymbol{\Omega} = \begin{Bmatrix} \Omega_i \\ 0 \\ 0 \\ 0 \\ 0 \end{Bmatrix} \tag{17}$$

where $\rho = \sum_{i=1}^{N_s} \rho_i$ is the mixture density.

In Eq. (16), n_x and n_y are the cartesian components of the unit outward normal vector. The system (16) is discretized according to a finite volume, cell-centered scheme. The physical space of the computational domain is divided into a certain number of cells or volumes, as shown in Fig. 1. Let the solution at time k for the n, m-cell be $W^k_{n,m}$, Fig. 1. The solution at time $k + 1$ may be determined by solving the discretized equation:

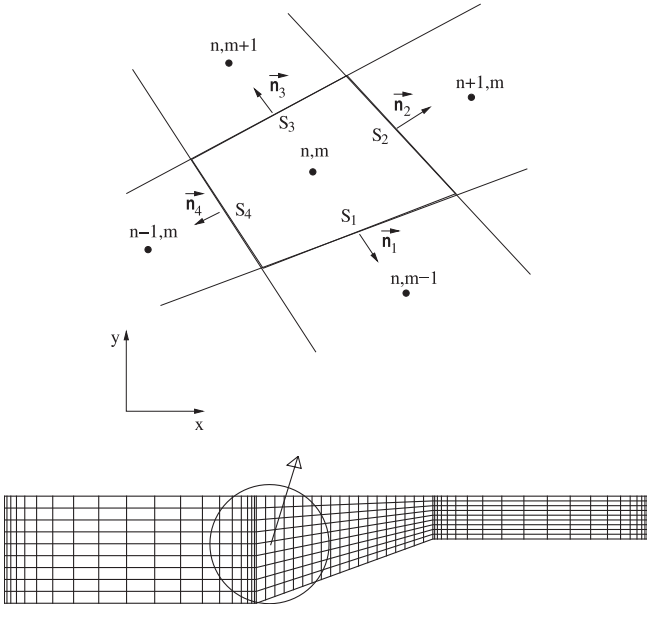

Fig. 1. Two-dimensional computational grid.

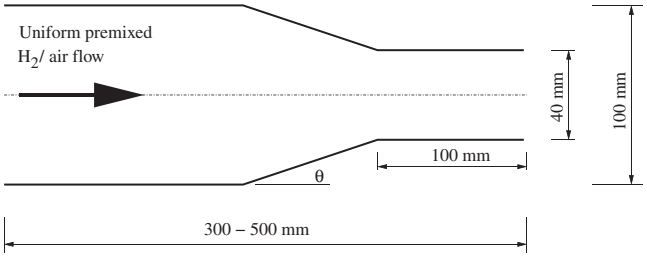

Fig. 2. Simplified wedge channel configuration.

$$\frac{d}{dt}(\mathcal{V}_{n,m}W_{n,m}) + \sum_{i=1}^{4}(F_i\mathcal{S}_i n_{x_i}) + \sum_{i=1}^{4}(G_i\mathcal{S}_i n_{y_i}) = \mathcal{V}_{n,m}\Omega_{n,m} \qquad (18)$$

where F_i and G_i are the fluxes in x and y direction computed at each cell interface ($i = 1,\ 2,\ 3,\ 4$) $\mathcal{S}_i$ is the corresponding cell surface and n_{x_i} and n_{y_i} are the components of the unit vector n normal to the cell interface. The integration in time is carried out according to a two-step Godunov scheme. At the *predictor* step, a standard first order flux difference splitting (FDS) scheme is used [9]: the conservative variables $\boldsymbol{W}$ are assumed as an averaged, constant value inside each cell. The fluxes $\boldsymbol{F}$ and $\boldsymbol{G}$ are evaluated by solving the Riemann's problems pertinent to the discontinuities that place at the interface of the cells. At the *corrector* level, the second order of accuracy is achieved by assuming a linear, instead of constant, behavior of the conserva-tive variables inside the cells, according to an essentially non-oscillatory (ENO) scheme [10]. The resulting scheme is second order accurate in both time and space. A semi-implicit integration procedure is used, to avoid numerical instability, to solve the chemical non-equilibrium for the mass conservation equations of the species [15]. Furthermore, the semi-implicit formulation allows a correct determination of the production term even in those flow fields where it changes very rapidly.

4. Model verification and results

In order to verify the numerical procedure described above a very complex, unsteady, supersonic combustion mechanism has been chosen as case-study. In particular, the normal detonation wave engine (NDWE) described in [3] has been considered for model verification. The chemical model used is based on a hydrogen-air combustion mechanism of seven species (H, O, OH,O_2, H_2, H_2OandN$_2$) and thirty-two reactions. The supersonic combus-tible mixture, is ignited by a shock/detonation wave in a simplified 2-D wedge channel representing the normal detonation wave engine. In this chemical model the species HO_2 and H_2O_2 are ne-glected and the N_2 is counted as a collisional partner in the ther-modynamic model and relaxation process, but it is not included in the chemical reaction model since the maximum temperature in the hydrogen-air reaction does not reach the dissociation temperature of nitrogen [11,12].

Tables A.1, A.2 (see Appendix A) report all the considered reactions with the chemical coefficients for the modified Arrhenius

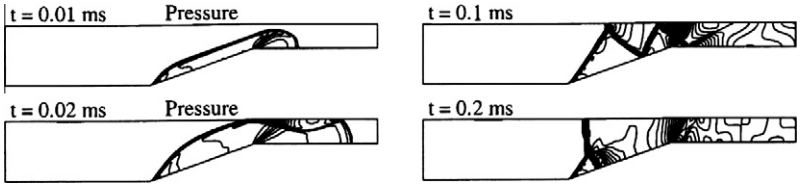

Fig. 3. Detonation wave at different times for $M_\infty = 4.5$ and $\Theta = 20^\circ$ [3].

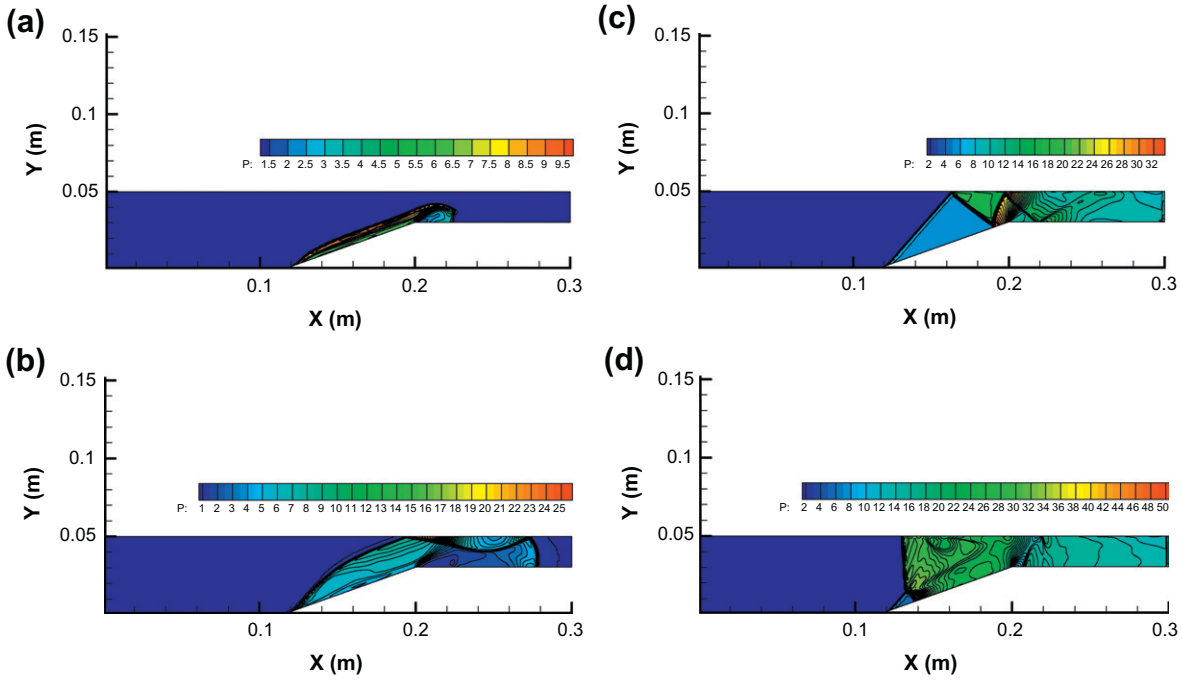

Fig. 4. Computed detonation wave at time t = 0.01, 0.02, 0.1, and 0.2 ms.

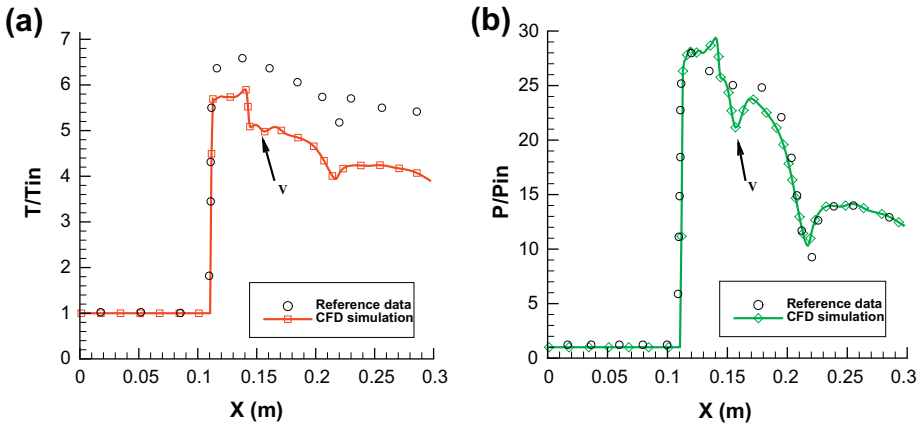

Fig. 5. Temperature and pressure comparison at time = 0.25 ms.

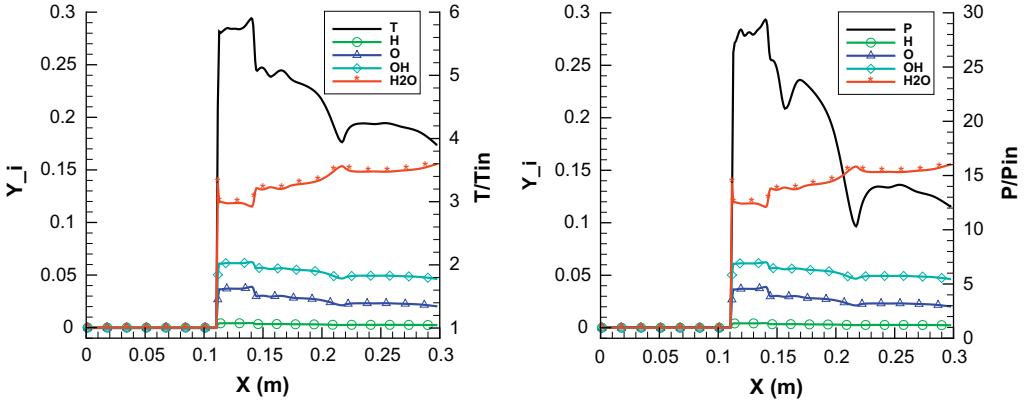

Fig. 6. Species concentration at time = 0.25 ms.

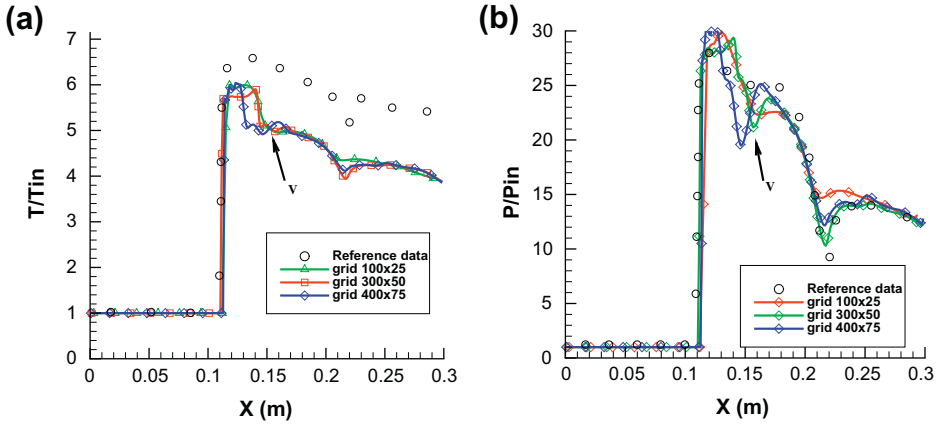

Fig. 7. Temperature and pressure comparison on different grids at time = 0.25 ms.

formula (10). α is an eventual multiplied factor which is added depending on the catalytic particle involved in the reaction. The other thermodynamic data needed in input are listed in Table A.3 [11].

The two-dimensional symmetric channel used for simulations is shown in Fig. 2. The channel consists of three sections: the rightmost parallel section is a nozzle for the exhaust flow, whereas the leftmost parallel section is the real combustion chamber. The crucial part of the channel is the wedge middle section which causes the ignition of the detonation process. The chosen wedge angle is $\theta = 20^{\circ}$, the channel height is 100 mm at the inlet and 40 mm at the outlet. The detonative flow is tested for an inlet Mach number of 4.5 with an inlet static pressure $p_{in} = 0.1$ MPa and static temperature $T_{in} = 700\ K$. The incoming supersonic flow is a premixed stoichiometric hydrogen-air mixture. The left boundary of the computational domain, which for the geometric symmetry enables only half of the flow to be simulated, is kept at the incoming flow conditions. The outflow boundary is modeled with non-reflective

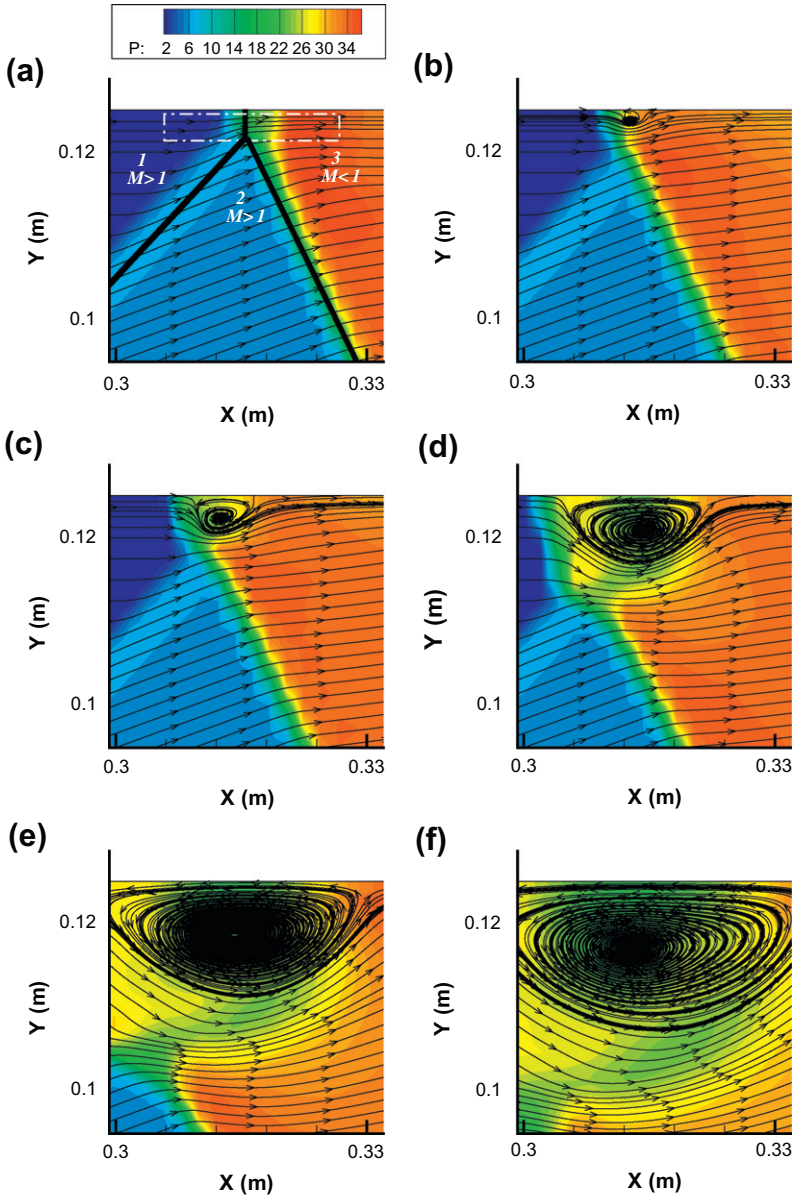

Fig. 8. Vortex-like structure formation and development at time t = 0.135, 0.140, 0.145, 0.150, 0.155, and 0.160 ms.

boundary conditions. At the symmetry plane, slip conditions are imposed. Moreover, to test code accuracy the computational domain has been discretized with three different grid size, i.e. 100 × 25, 300 × 50 and 400 × 75 points, respectively.

Recently, Shepherd [16], examining typical experimental data for a detonation wave has shown that the characteristic propagation distance is 1–10 m, while the reaction zone exhibits significant spatial gradient on the order of 1–10 μm. Despite the widespread availability of software for adaptive mesh refinement, this range of 10^7 in length scales poses a significant issue for accurate direct numerical simulation of the reactive flow with detailed chemical reaction kinetics.

In the tests presented the grid scale is on the order of 1000 μm, which is much larger than the one required by the reaction zone. This work only concerns the development of a methodology capable of quickly solving wave effects of detonation on the flow field in terms of pressure and temperature. For this reason, the grids used for the present calculation are much larger than those required for the accurate study of the combustion phenomena.

Fig. 4 shows the evolution of the detonation waves, plotting the isobars (p/p_{in}) of the corresponding detonative flow fields for different evolution times. For the considered conditions the temperature after the bow shock is high enough to ignite the mixture, thus a bow detonation wave is formed, attached to the wedge tip. The detonation is ignited at the very instant when the flow passes the wedge and consequently, as shown in Fig. 4a, the detonation kernel is already formed at t = 0.01 ms. Fig. 4b–d, shows the evolu-tion of the pressure field at time 0.02 ms, 0.1 ms and 0.2 ms, respectively. The presence of the wedge, followed by a straight sec-tion downstream, produces a complex flow field due to multiple shocks and expansion wave reflections, as shown in Fig. 4d, where a lambda shock is formed. The obtained results can be qualitatively compared with those reported in reference [3] in terms of wave pattern, Fig. 3.

Fig. 5 shows the computed non-dimensional temperature and pressure distributions along the symmetry plane at time t = 0.25 ms, where x = 0 is the left boundary, (Grid 300 × 50 points). In the case reported in Fig. 5 the detonation wave is prop-

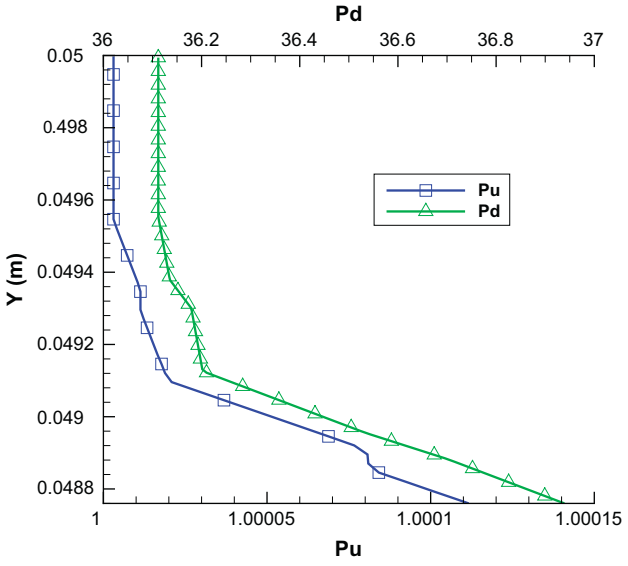

Fig. 9. Upstream (*Pu*) and downstream (*Pd*) pressure gradient in region 1 and 3.

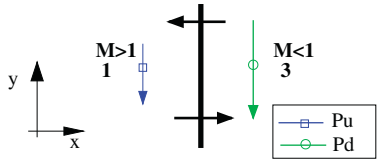

Fig. 10. Shock movement due to pressure gradient.

agating through the straight inlet section. High pressure and temperature are sustained for a large portion of this section, up to the wedge end, where these parameters are then affected by the expansion. The ability to sustain these high values for a fair period

Table A.1
Chemical reactions and arrhenius coefficients, [11].

n	Reaction	α	C [cm^3/(mol s)]	η	ϵ_0 [kJ/mol]
1	$H + O_2 \rightleftharpoons O + OH$	–	3.55×10^{15}	−0.40	69.45
2	$O + H_2 \rightleftharpoons H + OH$	–	5.08×10^{4}	2.70	26.32
3	$OH + H_2 \rightleftharpoons H + H_2O$	–	2.16×10^{8}	1.50	14.35
4	$O + H_2O \rightleftharpoons OH + OH$	–	2.97×10^{6}	2.00	56.07
5	$H_2 + H \rightleftharpoons H + H + H$	–	4.58×10^{19}	−1.40	436.75
6	$H_2 + O \rightleftharpoons H + H + O$	–	4.58×10^{19}	−1.40	436.75
7	$H_2 + OH \rightleftharpoons H + H + OH$	–	4.58×10^{19}	−1.40	436.75
8	$H_2 + O_2 \rightleftharpoons H + H + O_2$	–	4.58×10^{19}	−1.40	436.75
9	$H_2 + H_2 \rightleftharpoons H + H + H_2$	2.5	4.58×10^{19}	−1.40	436.75
10	$H_2 + H_2O \rightleftharpoons H + H + H_2O$	12.0	4.58×10^{19}	−1.40	436.75
11	$H_2 + N_2 \rightleftharpoons H + H + N_2$	–	4.58×10^{19}	−1.40	436.75
12	$O + O + H \rightleftharpoons O_2 + H$	–	6.16×10^{15}	−0.50	0.00
13	$O + O + O \rightleftharpoons O_2 + O$	–	6.16×10^{15}	−0.50	0.00
14	$O + O + OH \rightleftharpoons O_2 + OH$	–	6.16×10^{15}	−0.50	0.00
15	$O + O + O_2 \rightleftharpoons O_2 + O_2$	–	6.16×10^{15}	−0.50	0.00
16	$O + O + H_2 \rightleftharpoons O_2 + H_2$	2.5	6.16×10^{15}	−0.50	0.00
17	$O + O + H_2O \rightleftharpoons O_2 + H_2O$	12.0	6.16×10^{15}	−0.50	0.00
18	$O + O + N_2 \rightleftharpoons O_2 + N_2$	–	6.16×10^{15}	−0.50	0.00
19	$O + H + H \rightleftharpoons OH + H$	–	4.71×10^{18}	−1.00	0.00
20	$O + H + O \rightleftharpoons OH + O$	–	4.71×10^{18}	−1.00	0.00

of time may be attributed to the presence of the converging wedge section. Moreover, in the temperature and pressure distributions a vortex structure generated by the irregular shock reflection, that occurs during the transient, (indicated by *V* in Fig. 5) is evident. In Fig. 5a and b a comparison of the computed results with the same results reported in [3] is also shown. The computed temper-ature and pressure peak are different from the corresponding val-ues reported in [3] (lower temperature peak and higher pressure peak). These differences may be explained considering that the proposed method uses a more detailed chemical model, which also takes into account the water dissociation behavior. It should be

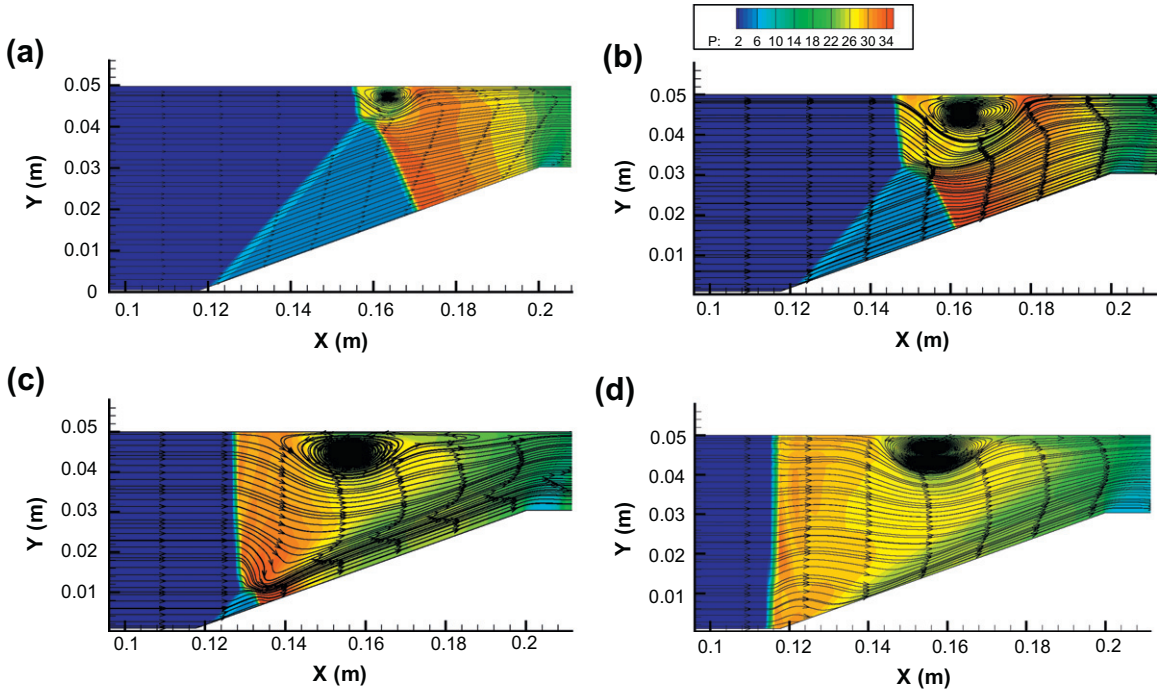

Fig. 11. Vortex-like structure developing and moving upstream the detonation wave at t = 0.12, 0.18, 0.22, and 0.25 ms.

Table A.2
Chemical reactions and arrhenius coefficients [11].

n	Reaction	α	$C[\mathrm{cm}^3/(\mathrm{mol\ s})]$	η	$\epsilon_0[\mathrm{kJ/mol}]$
21	$O + H + OH \rightleftharpoons OH + OH$	–	4.71×10^{18}	−1.00	0.00
22	$O + H + O_2 \rightleftharpoons OH + O_2$	–	4.71×10^{18}	−1.00	0.00
23	$O + H + H_2 \rightleftharpoons OH + H_2$	2.5	4.71×10^{18}	−1.00	0.00
24	$O + H + H_2O \rightleftharpoons OH + H_2O$	12.0	4.71×10^{18}	−1.00	0.00
25	$O + H + N_2 \rightleftharpoons OH + N_2$	–	4.71×10^{18}	−1.00	0.00
26	$H + OH + H \rightleftharpoons H_2O + H$	–	3.80×10^{22}	−2.00	0.00
27	$H + OH + O \rightleftharpoons H_2O + O$	–	3.80×10^{22}	−2.00	0.00
28	$H + OH + OH \rightleftharpoons H_2O + OH$	–	3.80×10^{22}	−2.00	0.00
29	$H + OH + O_2 \rightleftharpoons H_2O + O_2$	–	3.80×10^{22}	−2.00	0.00
30	$H + OH + H_2 \rightleftharpoons H_2O + H_2$	2.5	3.80×10^{22}	−2.00	0.00
31	$H + OH + H_2O \rightleftharpoons H_2O + H_2O$	12.0	3.80×10^{22}	−2.00	0.00
32	$H + OH + N_2 \rightleftharpoons H_2O + N_2$	–	3.80×10^{22}	−2.00	0.00

noted that the distribution of the species on the symmetry plane, Fig. 6, shows a decrease of water at the point of maximum heat and an increase of species H, O, OH. This process results in a lower peak temperature due to the dissociation of water. Consequently, the highest peak pressure can be justified by the greater number of dissociated molecules present in the mixture.

The influence of grid size on accuracy is also been tested and the results are presented in Fig. 7, showing a good consistency for the numerical method proposed.

As already mentioned, in these test conditions, an irregular shock reflection is originated. This reflection is particularly well captured by the numerical scheme, causing an inviscid flow separation and a vortex-like structure [17–19]. During the transient the interaction of the detonation wave with the oblique shock generates a triple point interaction, with the formation of an inviscid flow separation. Referring to Fig. 8a, region 1 is the supersonic inflow which is the isentropic region upstream of the shock, region 2 is the region downstream of the oblique wedge shock, and region 3 is the subsonic flow region downstream of the detonation wave. As highlighted in Fig. 8, the flow can be non-uniform: positive or negative pressure gradients y direction, $\partial p/\partial y$ can occur. In the simulation, due to the particular Mach and geometry conditions, there are negative pressure gradient at both sides of the detonation normal shock as the Rankine Hugoniot jump relationships also indicate (Fig. 9).

For this reason, the downstream subsonic flow will react to the pressure gradient, trying to reduce it by local compression or expansion: the subsonic region, therefore, will try to move as indicated in Fig. 10. In the proximity of the symmetry plane the shock will move upstream to strengthen shock and increase downstream pressure, and, far from the symmetry plane, it will move downstream to decrease downstream pressure. This movement changes the shock slope, leading to a shock that becomes more and more oblique and, as a consequence, weaker and weaker from the symmetry plane to the point of the triple interaction. As a consequence, a rotational flow takes place downstream of the shock and in some particular conditions, as in this case, it can lead to the generation of a vortex structure and to an inviscid flow separation. In Fig. 11 the evolution in time of this vortex structure downstream of the detonation wave is shown.

5. Conclusions

A computational method for the study of reacting flows in chemical non-equilibrium has been developed. The proposed numerical code is based on the calculation of the reacting equilibrium constant, based on Gibbs free energy and the Van't Hoff equation, and may be easily used for the simulation of any reacting mechanism with M_s reactions and N_s involved species. It simply needs to input the stoichiometric reaction constants, some thermochemical data and specific Arrhenius coefficients. The numerical code has been tested and verified with a hydrogen-air combustion mechanism of seven species and thirty-two reactions to simulate a supersonic combustible mixture, ignited by a shock/detonation wave in a simplified wedge channel, which represents a multi-mode detonation engine. The numerical results carried out by the present method show a suitable solution, and a good accuracy is demonstrated by the captured irregular shock interaction, due to the particular working conditions of the test case. For verification purposes a very detailed chemical model has been used. The chemical model takes into account the high temperature water dissociation behavior, which explains why, at the point of maximum heat, a decrease of water and an increase of species like H, O, OH can be observed. To improve the computational speed and to reduce the time consuming-effort, the presented code needs to be parallelized. It would also be suitable to implement viscous terms coupled with turbulence models in order allow particular geometries, involving cavities or injectors, to be dealt with. These modifications, if associated with an appropriate chemical model, will allow us to use the program to analyze several solutions for scramjet combustion chambers, in an attempt to optimize fuel consumption and predict and reduce NO_x emissions.

Table A.3 Thermodynamic data, [11].

Species	H	O	OH	O_2	H_2	H_2O	N_2
Number of moles	0	0	0	1	2	0	3.76
Molecular weight	1	16	17	32	2	18	28
$\Delta_f H^0(\mathrm{kJ/mol})$	217.999	249.173	38.987	0	0	−241.826	0
$\Delta_f G^0(\mathrm{kJ/mol})$	203.278	231.736	34.277	0	0	−228.921	0

6. Acknowledgements

This work was supported by the European Union, by the Regione Autonoma Valle d'Aosta and by the Ministero del Lavoro e delle Politiche Sociali (2011). The support from Regione Piemonte, with the grant RU/05/07-Bando-Ricerca-Scientifica-2006 is also gratefully acknowledged by the authors.

Appendix A. Chemical data

See Tables A.1–A.3.

References

[1] Munipalli R, Shankar V, Wilson DR, Kim H, Lu FK, Hagseth PE. A pulse detonation based multi-mode engine concept. AIAA paper 2001-1786; 2001.
[2] Wilson DR, Lu FK, Kim H, Munipalli R. Analysis of pulsed normal detonation wave engine concept. AIAA paper 2001-1784; 2001.
[3] Lu FK, Fan H, Wilson DR. Detonation waves induced by a confined wedge. J Aerosp Sci Technol 2006;10:679–85.
[4] Grismer P, Powers JM. Calculation for steady propagation of a generic ram configuration. J Propul Power 1995;11:105–11.
[5] Ashford SA, Emanuel G. Oblique detonation wave engine performance prediction. J Propul Power 1996;12:322–7.
[6] Brackett DC, Bogdonoff DW. Computational investigation of oblique detonation ramjet-in-tube concepts. J Propul Power 1996;12:322–7.
[7] Li C, Kailasanath K, Oran ES. Detonation structures behind oblique shocks. Phys Fluids 1994;6:1600–11.
[8] Winteberg E, Shepherd JE. The performance of steady detonation engines. AIAA paper 2003-0714; 2003.
[9] Pandolfi M. A contribution to the numerical prediction of unsteady flows. AIAA J 1983;22:37–46.
[10] Harten A, Henquist B, Osher S, Chackravarthy S. Uniformly high order accurate essentially nonoscillatory schemes-III. J Comput Phys 1987;71.
[11] Glassman I, Yetter RA. Combustion. 4th ed. Academic Press; 2008.
[12] Wesbrook CK, Dryner FL. Chemical kinetic modeling of hydrocarbon combustion. Progess Energy Combust Sci 1984;10.
[13] Pandolfi M. Physical aspects of hypersonic flow: fluid dynamics and non-equilibrium phenomena. The third joint Europe/U.S. short course in hypersonics, Aachen; 1990.
[14] Pandolfi M, Arina R, Botta N. Non-equilibrium hypersonic flows over corners. AIAA J 1991;29:241–53.
[15] Park C. On convergence of computation of chemically reacting flows. AIAA paper 85-0247; 1985.
[16] Sheperd JE. Detonation in gases. Proc Combust Inst 2009;32:83–98.
[17] Marsilio R. Vortical solutions in supersonic corner flows. AIAA J 1993;31:58–1651.
[18] Gun'ko YuP, Kudryavtsev AN, Rakhimov RD. Supersonic inviscid corner flows with regular and irregular shock interaction. J Fluid Dyn 2004;39:304–18.
[19] Nasuti F, Onofri M. Shock structure in separated nozzle flows. J Propul Power 2008;1:5–21.